Accepted Article

Title: Defect-Driven Enhancement of Electrochemical Oxygen Evolution on Co-Fe-Al Ternary Hydroxides

Authors: Yixuan Sun, Yuanyuan Xia, Long Kuai, Hongxia Sun, Wei Cao, Marko Huttula, Ari-Pekka Honkanen, Mira Viljanen, Simo Huotari, and Baoyou Geng

This manuscript has been accepted after peer review and appears as an Accepted Article online prior to editing, proofing, and formal publication of the final Version of Record (VoR). This work is currently citable by using the Digital Object Identifier (DOI) given below. The VoR will be published online in Early View as soon as possible and may be different to this Accepted Article as a result of editing. Readers should obtain the VoR from the journal website shown below when it is published to ensure accuracy of information. The authors are responsible for the content of this Accepted Article.

To be cited as: *ChemSusChem* 10.1002/cssc.201900831

Link to VoR: http://dx.doi.org/10.1002/cssc.201900831

COMMUNICATION

Defect-Driven Enhancement of Electrochemical Oxygen Evolution on Co-Fe-Al Ternary Hydroxides
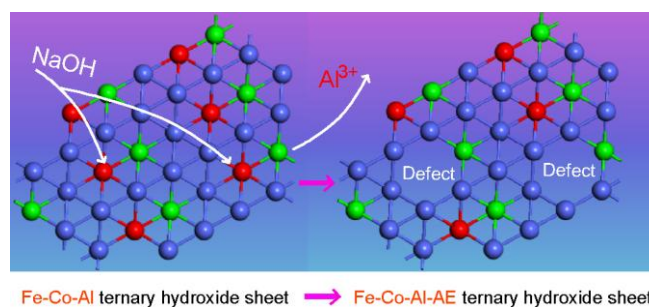
Yixuan Sun[a], Yuanyuan Xia[a], Long Kuai[a], Hongxia Sun[a], Wei Cao[b], Marko Huttula[b], Ari-Pekka Honkanen[c], Mira Viljanen[c], Simo Huotari[c] and Baoyou Geng*[a]

Abstract: Efficient, abundant and low-cost catalysts for oxygen evolution reaction (OER) are required in energy conversion and storage. This paper reports a doping-etching route to access defect rich Co-Fe-Al (Co-Fe-Al-AE) ternary hydroxide nanosheets for superior electrochemical oxygen evolution. After partially etching of Al, the ultrathin $Fe_3Co_2Al_2$–AE electrocatalysts with a rich pore structure are obtained with a change of cobalt valence state shift towards higher valence ($Co^{2+} \rightarrow Co^{3+}$), along with substantial improvements of catalytic performance. The Fe_3-Co_2-Al_2-AE shows a notably lower overpotential of only 284 mV at a current density of 10 mA/cm^2, and a 2-fold higher OER mass activity than that of the etching-free Fe_3-Co_2-Al_2 with an overpotential of 350 mV. The density functional theory result shows the leaching of Al changes the OER rate determine step. The overpotential undergoing the step of *OOH to O_2 on Fe_3-Co_2-Al_2 is switched to formation of OOH from *O on the Al defective catalysts. This work demonstrates an effective route to design and synthesize transition metal electrocatalyst, and provides a promising alternative prospect for further development of oxygen evolution catalysts.

Up to date, transition-metal-based catalysts have provided insights into the application in many fields, including energy conversion and storage.[1] Moreover, oxygen evolution reaction[2] (OER) represents one of the most promising processes toward energy concerns. As a half reaction of water splitting, oxygen is produced via several proton/electron coupled procedures.[3] Owing to the high efficiency and environmental friendliness, transition-metal materials have lately received great attentions as OER catalysts.[4] More recently, numerous types of transition-metal-based catalysts, such as sulfides,[5] oxides[6] and (oxy)hydroxide,[7] have provided a promising alternative to solve the problem of OER. Extensive efforts have been dedicated to morphological controls to enlarge active sites on the Co-, Ni- and Fe-based OER catalysts.[8] The more exposed structures enable the fast diffusion of reactants and rapid proton-coupled electron to transfer the products.[9] Two-dimensional (2D) catalytic active sites are easily available and give rise to a good electrocatalytic activity.[10] Thus, 2D transition-metal-based catalysts have been the attractive glamour.

It was reported that the single-atom Au supported on layered double hydroxides (LDH) is helpful to enhance OER activity of current electrocatalysts.[11] Au could transfer electrons to the surface of LDH, changing the charge distribution and thus further improving the catalytic performance. To overcome high cost and server scarcity of Au, researches have been focused on alternative materials employing two or more different transition metals and creating a mixed-transition metal 2D nanomaterials, such as Ni-Fe,[12] Co-Fe,[13] Ni-Fe-Co,[14] Ni-Fe-Al[15] etc. By doping hetero-components, a catalyst may be engineered so that benefits of individual element are retained while its drawbacks eliminated. Bates et al. demonstrated that the charge-transfer effects of the Co component in the Ni-Fe-Co MMO have been studied in their ability to facilitate oxidation of the insulating $Ni(OH)_2$ to the conductive NiOOH, thus activating the Fe sites in the conductive Ni/Co-oxide host at lower overpotential.[16] Among those strategies, elemental doping has generally been proved to modulate the oxygen vacancies.[17] The effect of oxygen vacancies on OER is believed to be related to the OER mechanism, where naked or unsaturated metal sites served as active sites.[18] Therefore, it has been of great scientific significance to explore the essential changes in materials caused by structural defects, so as to further understand the root of the influence of defects on catalytic performance. There are not many existing literatures that may be involved in the process of original inquiry, and it is worthwhile devoting much effort to this.

[a] Ms. Y. Sun, Y. Xia, Dr. L. Kuai, Ms. H. Sun, and Prof. Dr. B. Geng
College of Chemistry and Materials Science, The Key Laboratory of Functional Molecular Solids, Ministry of Education, Anhui Laboratory of Molecular-Based Materials, The Key Laboratory of Electrochemical Clean Energy of Anhui Higher Education Institutes, Anhui Normal University
NO.189 South Jiuhua Road, Wuhu, 241002 (P. R. China).
E-mail: bygeng@mail.ahnu.edu.cn
[b] Prof. W. Cao, M. Huttula
Nano and Molecular Systems Research Unit, University of Oulu, P.O. Box 3000, FIN-90014 Oulu, Finland
[c] Mr. A. Honkanen, Ms. M. Viljanen, and Prof. S. Huotari
Department of Physics, University of Helsinki, PO Box 64, FI-00014 Helsinki, Finland

Supporting information for this article is given via a link at the end of the document.((Please delete this text if not appropriate))

Scheme 1. The synthesis illustration of defect rich Fe-Co-Al-AE ternary hydroxide sheets.

In this work, as illustrated in Scheme 1, we developed a leaching strategy to obtain a defect rich Fe-Co-Al-AE ternary hydroxide sheets (marked as Fe-Co-Al-AE for short) for notably enhanced OER performance in alkaline media. The Fe-Co-Al-AE materials are obtained by partially leaching Al from Fe-Co-Al with NaOH. Moreover, partially etching Al resulted in the porous $Fe_3Co_2Al_2$–AE electrocatalysts with a shifted valance state of Co from +2 to +3. The catalytic performance is substantially

improved. The Fe_3-Co_2-Al_2-AE shows a notably lower overpotential of only 284 mV at a current density of 10 mA/cm^2, and a 2-fold higher OER mass activity than that of the etching-free Fe_3-Co_2-Al_2 with an overpotential of 350 mV. The physical mechanisms leading to the unique electrochemical behaviour have been explored through density functional theory (DFT) along with experimental determinations of electronic structures. Therefore, this work not only develops an efficient OER materials, but also deepen the knowledge of defect on OER processes.

The synthesis of Fe-Co-Al-AE ternary hydroxide nanosheets (marked as Fe-Co-Al-AE for short) are produced from Fe-Co-Al ternary hydroxide nanosheets (marked as Fe-Co-Al for short) by leaching partial lattice Al with NaOH. Herein, we show a case study of Fe_3-Co_2-Al_x-AE nanosheets. Compared with microflower Fe_3-Co_2-Al_2 (Figure 1a), the morphology of Fe_3-Co_2-Al_x-AE changes to loosen and broken nanomeshes (Figure 1e) after 48 hours' strong continuous leaching of Al. Moreover, the TEM and HAADF-STEM images show that the structure of Fe_3-Co_2-Al_x-AE (Figure 1f and g) becomes microporous while Fe_3-Co_2-Al_2 (Figure 1b and c) is smooth nanosheets. The abundant micropores may be derived from the aluminum leaching process. According to the EDS analysis (Figure S1), the Al proportion decreases to 2% from 8% and most Al are leached out from the

lattice form Fe_3-Co_2-Al_2 sheets. The elemental EDS mappings of Fe_3-Co_2-Al_2 (Figure 1d) and Fe_3-Co_2-Al_2-AE (Figure 1h) are performed to investigate the leached amount of Al. Obviously, the relative intensity of Al/Co get weaken. Combined with the inductively coupled plasma test (ICP) test data(Table S1), it can be seen that the content of aluminum is indeed significantly reduced. Besides, the crystal structure is well maintained based on the powder X-ray diffraction (XRD) patterns (Figure S2) of Fe_3-Co_2-Al_2 and Fe_3-Co_2-Al_2-AE nanosheets, which are all indexed to the LDH patterns (PDF# 14-0558). It has been confirmed by many other research groups that amorphous structures show stronger activity than crystalline structures. The products herein are thin 2D nanosheets and the crystallinity is very weak, which had also a certain impact on the improvement of electrochemical catalytic performance.[10,19] In addition, the Brunauer Emmett Teller (BET) specific surface area of Fe_3-Co_2-Al_2 and Fe_3-Co_2-Al_2-AE were assessed with N_2 adsorption/desorption isotherms, so as to evaluate the changes of specific surface area before and after etching.[20] The BET specific surface area of Fe_3-Co_2-Al_2-AE is 307 m^{2}g^{-1}, which is much larger than that of Fe_3-Co_2-Al_2 (120 m^{2}g^{-1}; Figure S5). Clearly, more active sites can be provided for OER through the aluminum leaching process.
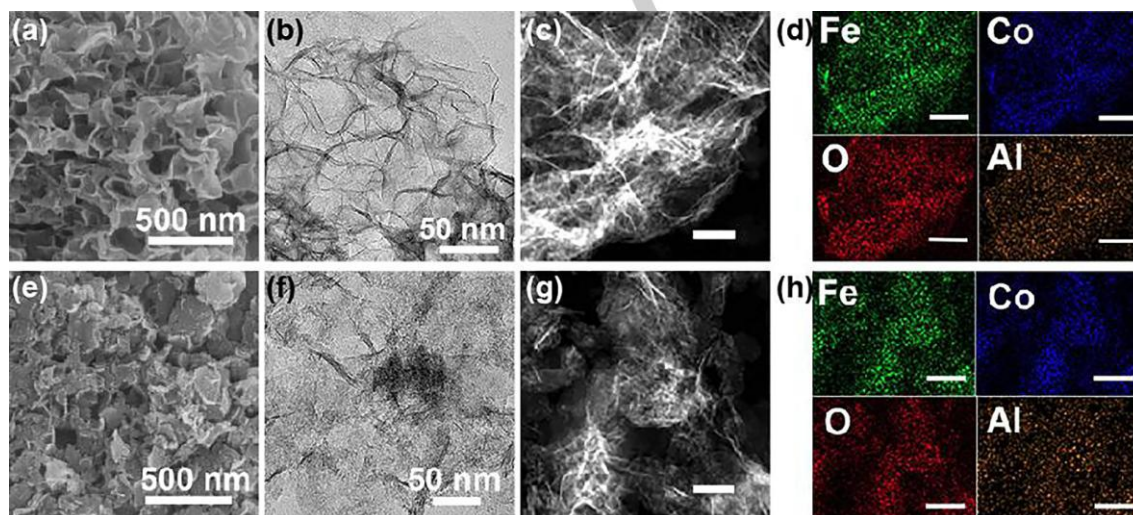

Figure 1. SEM (a, e), TEM (b, f), HAADF-STEM (c, g) and EDS-mapping (d, h) images of Fe_3-Co_2-Al_2 (a to d) and Fe_3-Co_2-Al_2-AE (e-h) hydroxide nanosheets. The scale bars for Figure 1c, d, g and h are 20 nm.

X-ray photoelectron spectroscopy (XPS) was performed to offer insights of the chemical environment of Fe_3-Co_2-Al_2 (Figure 2a) and Fe_3-Co_2-Al_2-AE (Figure 2b). As shown in Figure 2c and d, the chemical state of Fe barely changes after leaching of Al. While, the chemical state of Co changes notably. According to the fitted spectra (Figure 2e and f), dominant Co^{III} species appear after partially leaching of Al. The surface chemical environment change is also indicated from the O 1s spectrum (Figure 2g and h). There are two O species in Fe_3-Co_2-Al_2, which shows a strong peak at 530.8 eV (OH$^-$) and a weak peak at 528.9 eV (O^{2-})[21]. Two strong peaks peaks at 530.3 eV (OH-)

and 528.9 eV (O^{2-}) in Fe_3-Co_2-Al_2-AE are attributed to the effect of interactions between surface hydroxyl groups and metal ions. In the etched samples, adsorbed oxygen species exists much more in the form of O^{2-}, indicating that the existence form of other ions in its vicinity changes simultaneously. More importantly, apparent adsorbed molecule H_2O located at 531.5 eV are found in the surface of Fe_3-Co_2-Al_2-AE, which contributes activation of H_2O for oxygen evolution.

X-ray absorption near-edge structure (XANES) spectroscopy was further performed to probe the local atomic structure of Co and Fe in Fe_3-Co_2-Al_2 and Fe_3-Co_2-Al_2-AE. Different from surface

sensitive XPS, the XAS probes the overall chemical environment within the microporous samples.[22] For meaningful comparison, we also studied Fe_3-Co_2 hydroxide nanosheets. As shown in Figure 3a, the corresponding Co K-edge spectra of Fe_3-Co_2 and Fe_3-Co_2-Al_2 are similar with the $CoCO_3$ (Co^{2+}), while the Fe_3-Co_2-Al_2–AE spectrum is located closely to that of the Co_3O_4 references.[23] It implies that the Co ions are present in a mixed Co^{2+} and Co^{3+} oxidation state, indicating a higher average Co oxidation state after partially etching, which is well consistent with the results of XPS data. As for the XANES of the Fe K-edge (Figure 3c and d), the peaks for Fe_3-Co_2, Fe_3-Co_2-Al_2 and Fe_3-Co_2-Al_2-AE are all located closely to each other, indicating the close state of Fe in the above three samples. It well agrees with the results of XPS study.
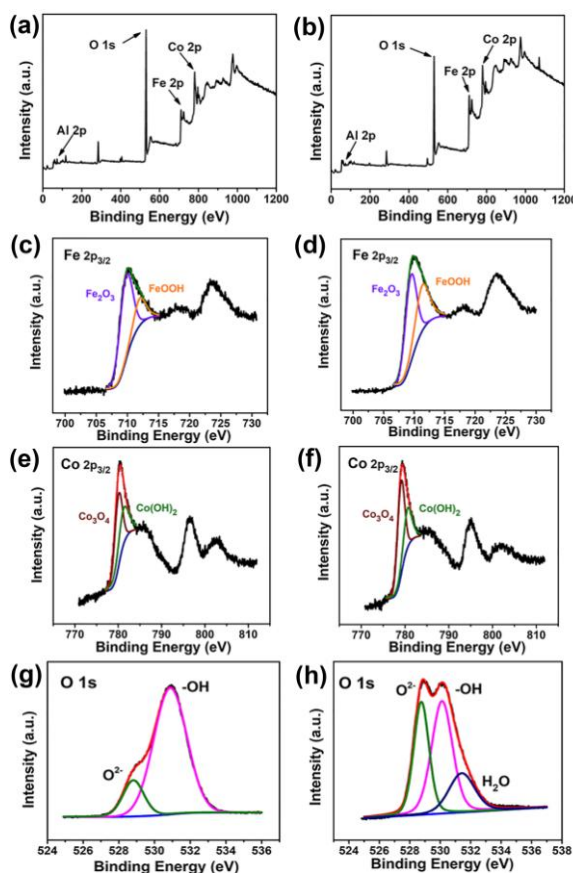

Figure 3. (a) Co K-edge XANES spectra of Fe_3-Co_2, Fe_3-Co_2-Al_2 and Fe_3-Co_2-Al_2–AE with references to Co_3O_4, $CoCO_3$ and $LiCoO_2$; (b) the expanded XANES ranging from 7704 to 7716 eV; (c) Fe K-edge XANES spectra of Fe_3-Co_2, Fe_3-Co_2-Al_2 and Fe_3-Co_2-Al_2–AE; (d) expanded XANES ranging from 7108 to 7120 eV.

Figure 2. XPS surveys of Fe_3-Co_2-Al_2 (a) and Fe_3-Co_2-Al_2–AE (b), fitted Fe fine XPS spectra of Fe_3-Co_2-Al_2 (c) and Fe_3-Co_2-Al_2–AE (d), fitted Co fine XPS spectra of Fe_3-Co_2-Al_2 (e) and Fe_3-Co_2-Al_2–AE (f) and fitted O fine XPS spectra of Fe_3-Co_2-Al_2 (g) and Fe_3-Co_2-Al_2–AE (h).

In order to evaluate the oxygen-evolving performance, electrochemical measurements were conducted with catalyst loading of 200 µg/cm^2 on the glassy carbon (GC) electrode. Cyclic voltammetry was recorded in an O_2-saturated 1.0 M KOH solution. To depict the change trend of electrocatalytic performance more intuitively, we carried out the OER LSV curves at the scanning speed of 10 mV/s. The Fe_3-Co_2 hydroxide nanosheets were chosen as the reference to investigate the performance of Fe_3-Co_2-Al_x and Fe_3-Co_2-Al_x-AE
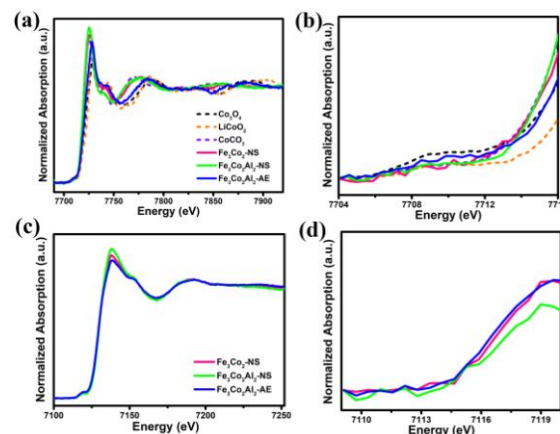
because Fe_3-Co_2 presented best OER activity (Figure S6). Previous results demonstrate the elemental doping is an effective approach to adjust the coordination chemical environment of electrocatalysts.[24] As shown in Figure 4a, the introduction of trivalent aluminum ions has greatly affected the chemical environment of the Fe_3-Co_2 with defects or vacancies, thus increasing the active sites of the catalyst. At the same time, it has been more extensive interlaminar space and enhanced the electron mass transfer performance between active materials, and then it shows better OER catalytic activity than binary Fe_3-Co_2 hydroxide nanosheets. The optimized proportion of Fe-Co-Al is Fe_3-Co_2-Al_2. More interestingly, as shown in Figure 4b, the OER activity get further increased for Fe_3-Co_2-Al_x-AE. Typically, the OER overpotential in Fe_3-Co_2-Al_2-AE is 284 mV in a current density of 10 mA/cm^2, much lower than that in Fe_3-Co_2 (397 mV). Moreover, as shown in Figure 4c, the improvement is general to all the Fe-Co-Al-AE samples in comparison with the materials without Al leaching.

Tafel slope is another important factor for evaluating the catalytic kinetics, as is shown in Figure S6a and b. The slope of the final product ultrathin Fe_3-Co_2-Al_2-AE was 100.6 mV/dec, while the slope of Fe_3-Co_2 and Fe_3-Co_2-Al_2 is 122.7 and 111.9 mV/dec, respectively. The change of the electrochemical impedance spectroscopy (EIS, Figure S7c and d) is consistent with the above analysis. The Faradic resistance of Fe_3-Co_2-Al_2-AE was 490 Ω (at a working potential of 0.45V), lower than both Fe_3-Co_2 and Fe_3-Co_2-Al_2. The long-term stability (Figure S8) of $Fe_3Co_2Al_2$–AE was obtained by chronoamperometric measurements in 1 M KOH solution. The stability of the material can hold 5.5 hours. Surprisingly, the OER mass activity (Table S2) of the $Fe_3Co_2Al_2$–AE is 48 times that of Fe_3-Co_2, 2.35 times that of Fe_3-Co_2-Al_2 at an overpotential of 350 mV.[25]
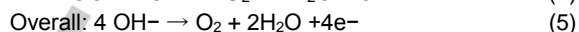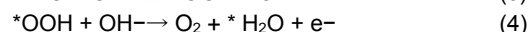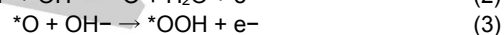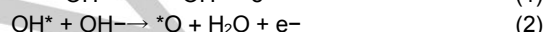
COMMUNICATION

WILEY-VCH
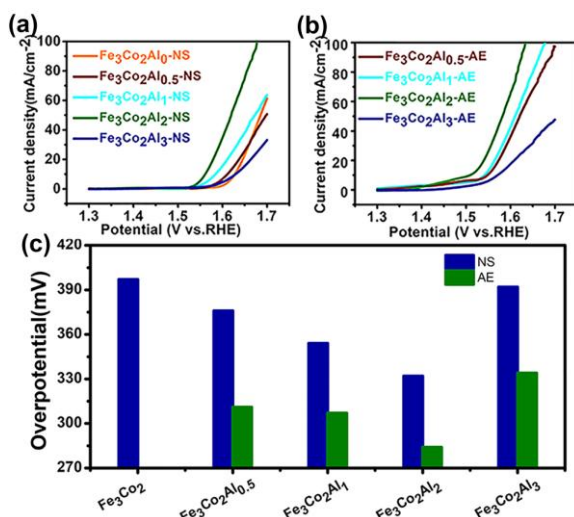
Figure 4. LSV curves of Al doping amount dependent OER of Fe-Co-Al nanosheets (a) and their performance after Al leaching of Fe-Co-Al nanosheets (b), and the overpotential summary (c) derived from OER polarization curves at current density of 10 mA/cm^2. All measurements were performed in O$_2$-saturated 1.0 M KOH.

Stability is a also key factor for evaluating the catalyst. Some materials cannot maintain their integrety during the electrochemical reaction.[26] In our case, after the cyclic stability test, the morphology and structural integrity of the electrode samples are well maintained without obvious damage. As shown in the SEM and TEM images (Figure S9), the prepared samples still retain the flaky structure. In addition, the XRD study shows a similar crystal structure to that before the test (Figure S10). It is found from XPS data (Figure S11) that there is no significant change in Fe before and after etching, while Co could still be found in the coexistence of two kinds of valence state. The results indicate that the structure integrity of the sample is well maintained during the cycle.

To understand the defect-driven enhancement of Fe$_3$-Co$_2$-Al$_2$-AE, the OER processes were calculated by density functional theory at GGA+U level. Three U values determined by samples were studied in this work, shown as insets of Figure 5b. The mechanism of OER in alkaline media developed by Nørskov[27] consist of four one-electron reactions:

$$OH^- + * \rightarrow OH* + e^- \quad (1)$$
$$OH* + OH^- \rightarrow *O + H_2O + e^- \quad (2)$$
$$*O + OH^- \rightarrow *OOH + e^- \quad (3)$$
$$*OOH + OH^- \rightarrow O_2 + *H_2O + e^- \quad (4)$$
$$\text{Overall: } 4OH^- \rightarrow O_2 + 2H_2O + 4e^- \quad (5)$$

The Gibbs free energy change of each reaction is calculated by the equation:

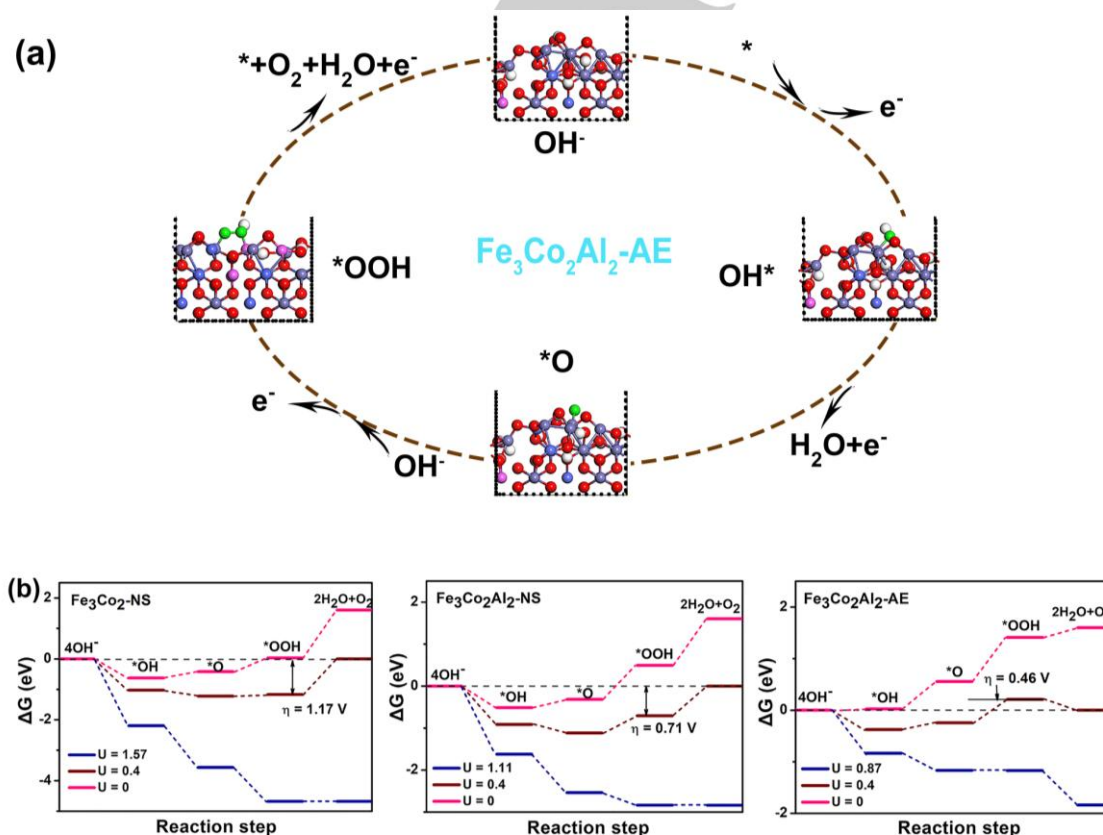$$\Delta G_i = \Delta E_i + \Delta ZPE_i - T\Delta S_i - eU \quad (6)$$

Figure 5. (a) OER mechanism on Fe$_3$-Co$_2$-Al$_2$-AE; (b) The calculated free energy on Fe$_3$-Co$_2$, Fe$_3$-Co$_2$-Al$_2$ and Fe$_3$-Co$_2$-Al$_2$-AE surfaces for OER processes.

COMMUNICATION

WILEY-VCH

where ∆E is the total energy change between reactants and products obtained by DFT calculations; ∆ZPE is the change of zero-point energy; ∆S denotes the change of entropy. i represents the intermediates of OH, O and OOH; U is the potential measured against normal hydrogen electrode (NHE) at standard conditions; e is the transferred charge; T is the temperature with unit K). In here, T = 300 K is considered.

Figure 5a illustrates each step of the end product in the OER reaction process. In Figure 5b, Gibbs free energy images of OER response processes at different potentials are given for three samples respectively. As can be seen from Figure 5b, the overpotential depends on the level of outlying potential expressed in the step from *OOH to O_2 for both Fe_3-Co_2 and Fe_3-Co_2-Al_2 while it changes to the formation of *OOH from *O for Fe_3-Co_2-Al_2-AE. As a result, the activation barrier of OER on Fe_3-Co_2-Al_2-AE is as low as 0.46 eV, which is much lower than Fe_3-Co_2-Al_2 (0.71 eV) and Fe_3-Co_2 (1.17eV). The result is well consistent with the observation of OER performance in 1.0 M KOH.

In summary, this paper demonstrates an efficient doping-etching route to access defect rich Co-Fe-Al-AE ternary hydroxide nanosheets for superior electrochemical oxygen evolution. The Fe_3-Co_2-Al_2-AE shows a notably lower overpotential of only 284 mV at a current density of 10 mA/cm2, and a 2-fold higher OER mass activity than that of the etching-free Fe_3-Co_2-Al_2 at 350 mV. The DFT points out that the Al defects change the OER rate-determine step (RDS) that overpotential depends on the step of *OOH to O_2 for Fe_3-Co_2-Al_2 while it changes to the formation of *OOH from *O for Fe_3-Co_2-Al_2-AE. In the future, the oxygen-evolving investigated in this work could represent a crucial and effective method to purposely create vacancy defects on the surface of a material and enhance its catalytic activity for specific reactions.

[1] a) H. Osgood, S. V. Devaguptapu, X. Hui, J. Cho, W. Gang, *Nano Today* **2016**, 11, 601-625; b) C. Xu, X. Guo, T. Zheng, G. Ji, H. Ning, Y. Zhang, *J. Mater. Chem. A* **2018**, 6, 10243-10252; c) Z. Yan, L. Hu, S. Zhao, L. Wu, *Adv. Funct. Mater.* **2016**, 26, 4085-4093.

[2] a) J. Geng, L. Kuai, E. Kan, Y. Sang, B. Geng, *Chem. Eur. J.* **2016**, 22, 14480-14483; b) S. He, Y. Huang, J. Huang, W. Liu, T. Yao, S. Jiang, F. Tang, J. Liu, F. Hu, Z. Pan, Q. Liu, *J. Phys. Chem. C* **2015**, 119, 26362-26366; d) W. Wang, L. Kuai, W. Cao, M. Huttula, S. Ollikkala, T. Ahopelto, A. P. Honkanen, S. Huotari, M. Yu, B. Geng, *Angew. Chem. Int. Ed.* **2017**, *56*, 14977-14981.

[3] M. Tahir, P. Lun, F. Idrees, X. Zhang, W. Li, J. J. Zou, L. W. Zhong, *Nano Energy* **2017**, 37, 136-157; b) H. Wang, J. Wang, Y. Pi, Q. Shao, Y. Tan, X. Huang, *Angew. Chem. Int. Ed.* **2019**, *58*, 2316-2320

[4] L. Han, S. Dong, E. Wang, *Adv. Mater.* **2016**, 28, 9266-9291; b) Y. Zhang, B. Ouyang, J. Xu, G. Jia, S. Chen, R. S. Rawat, H. J. Fan, *Angew. Chem. Int. Ed.* **2016**, *55*, 8670-8674.

[5] Y. Liu, Q. Li, R. Si, G. D. Li, W. Li, D. P. Liu, D. Wang, L. Sun, Y. Zhang, X. Zou, *Adv.Mater.* **2017**, 29, 1606200.

[6] Y. Zhao, X. Jia, G. Chen, L. Shang, G. I. Waterhouse, L. Z. Wu, C. H. Tung, D. O'Hare, T. Zhang, *J. Am. Chem. Soc.* **2016**, 138, 6517-6524.

[7] a) L. Feng, A. Li, Y. Li, J. Liu, L. Wang, L. Huang, Y. Wang, X. Ge, *Chempluschem* **2017**, 82, 483-488; b) J. Ping, Y. Wang, Q. Lu, B. Chen, J. Chen, Y. Huang, Q. Ma, C. Tan, J. Yang, X. Cao, Z. Wang, J. Wu, Y. Ying, H. Zhang, *Adv. Mater.* **2016**, 28, 7640-7645; c) L. Zeng, L. Yang, J. Lu, J. Jia, J. Yu, Y. Deng, M. Shao, W. Zhou, *Chin. Chem. Lett.* **2018**, 29, 1875-1878.

[8] W. Zhang, K. Zhou, *Small* **2017**, 13, 1700806.

[9] Y. Liu, H. Cheng, M. Lyu, S. Fan, Q. Liu, W. Zhang, Y. Zhi, C. Wang, C. Xiao, S. Wei, *J. Am. Chem. Soc.* **2014**, 136, 15670-15675; b) D. Chen, M. Qiao, Y. R. Lu, L. Hao, D. Liu, C. L. Dong, Y. Li, S. Wang, *Angew. Chem. Int. Ed.* **2018**, *57*, 8691-8696.

[10] a) Y. Li, F. M. Li, X. Y. Meng, S. N. Li, J. H. Zeng, Y. Chen, *ACS Catal.* **2018**, 8, 1913-1920; b) C. Tan, X. Cao, X. Wu, Q. He, J. Yang, X. Zhang, J. Chen, W. Zhao, S. Han, G. Nam, M. Sindoro, H. Zhang, *Chem. Rev.* **2017**, 117, 6225-6331.

[11] J. Zhang, J. Liu, L. Xi, Y. Yu, N. Chen, S. Sun, W. Wang, K. M. Lange, B. Zhang, *J. Am. Chem. Soc.* **2018**, 140, 3876-3879.

[12] F. Dionigi, P. Strasser, *Adv. Energy Mater.* **2016**, 6, 1600621.

[13] X. Ming, D. G. Ivey, *Electrochim. Acta* **2017**, 260, 872-881.

[14] D. Zhou, C. Zhao, X. Lei, W. Tian, Y. Bi, J. Yin, N. Han, T. Gao, Z. Qian, K. Yun, *Adv. Energy Mater.* **2017**, 8, 1701905.

[15] H. Liu, Y. Wang, X. Lu, H. Yi, G. Zhu, R. Chen, L. Ma, H. Zhu, Z. Tie, L. Jie, *Nano Energy* **2017**, 35, 350-357.

[16] M. K. Bates, Q. Jia, H. Doan, W. Liang, S. Mukerjee, *ACS Catal.* **2016**, 6, 155-161.

[17] J. Xie, X. Zhang, H. Zhang, J. Zhang, S. Li, R. Wang, B. Pan, Y. Xie, *Adv. Mater.* **2017**, 29, 1604765.

[18] D. Zhou, X. Xiong, Z. Cai, N. Han, Y. Jia, Q. Xie, X. Duan, T. Xie, X. Zheng, X. Sun, X. Duan, *Small Methods* **2018**, 2, 1800083.

[19] a) Y. Xue, Z. Ren, Y. Xie, S. Du, J. Wu, H. Meng, H. Fu, *Nanoscale* **2017**, 9, 16256-16263; b) J. Wu, Z. Ren, S. Du, L. Kong, B. Liu, W. Xi, J. Zhu, H. Fu, *Nano Res.* **2016**, 9, 713–725.

[20] a) Y. Chen, X. Li, K. Park, W. Lu, C. Wang, W. Xue, F. Yang, J. Zhou, L. Suo, T. Lin, H. Huang, J. Li, J. B. Goodenough, *Chem,* **2017**, 3, 152-163; b) M. Wang, C. Tang, C. Ye, J. Duan, C. Li, Y. Chen, S. Bao, M. Xu, *J. Mater. Chem. A,* **2018**, 6, 14734-14741.

[21] S. Hao, B. Zhang, J. Feng, Y. Liu, S. Ball, J. Pan, M. Srinivasan, Y. Z. Huang, *J. Mater. Chem. A* **2017**, 5, 8510-8518.

[22] a) L. Zhuang, Y. Jia, H. Liu, X. Wang, R. K. Hocking, H. Liu, J. Chen, L. Ge, L. Zhang, M. Li, C. Dong, Y. Huang, S. Shen, D. Yang, Z. Zhu, X. Yao, *Adv. Mater.* **2019**, 31, 1805581; b) R. K. Hocking, R. Brimblecombe, L. Chang, A. Singh, M. H. Cheah, C. Glover, W. H. Casey, L. Spiccia, *Nature Chem.*, **2011**, 3, 461–466.

[23] J. G. Kim, Y. Kim, Y. Noh, W. B. Kim, *Chemsuschem* **2015**, 8, 1752-1760.

[24] J. L. Lado, X. Wang, E. Paz, E. Carbo-Argibay, N. Guldris, C. Rodríguez-Abreu, L. Liu, K. Kovnir, Y. V. Kolen'ko, *ACS Catal.* **2015**, 5, 6503−6508.

[25] L. Zhuang, J. Yi, T. He, A. Du, X. Yan, G. Lei, Z. Zhu, X. Yao, *Nano Res.* **2018**,11, 3509-3518.

[26] B. Qu, L. Yuan, J. Li, J. Wang, H. Lv, X. Yang, *J. Mater. Chem. A* **2019**, 7, 150-156.

[27] a) J. Greeley, T. F. Jaramillo, J. Bonde, I. B. Chorkendorff, J. K. Nørskov, *Nature Materials* **2006**, 5, 909-913; b) J. K. Nørskov, J. Rossmeisl, A. Logadottir, L. Lindqvist, J. R. Kitchin, T. Bligaard, H. J. K. Jonsson, *J. Phys. Chem. B* **2004**, 108, 17886-17892; c) J. Rossmeisl, Z. W. Qu, H. Zhu, G. J. Kroes, J. K. Nørskov, *J. Electroanal Chem.* **2007**, 607, 83-89.

COMMUNICATION

Entry for the Table of Contents

COMMUNICATION
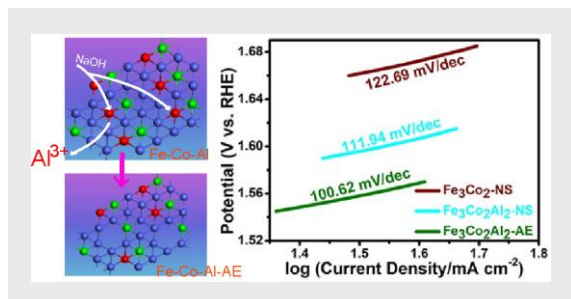
Yixuan Sun, Yuanyuan Xia, Long Kuai, Hongxia Sun, Wei Cao, Marko Huttula, Ari-Pekka Honkanen, Mira Viljanen, Simo Huotari and Baoyou Geng*

Page No. – Page No.

Defect-Driven Enhancement of Electrochemical Oxygen Evolution on Co-Fe-Al Ternary Hydroxides

This work presents a doping-etching route to access defect rich ultrathin Co-Fe-Al (Co-Fe-Al-AE) ternary hydroxide nanosheets for superior electrochemical OER. The Al-defects of $Fe_3Co_2Al_2$–AE boost cobalt valence state to shift towards higher valence, along with the catalytic performance improvement greatly. The Fe_3-Co_2-Al_2-AE shows a 2-fold higher OER mass activity than that of the defect-free Fe_3-Co_2-Al_2 under an overpotential of 350 mV.